J Mater Sci: Mater Electron **(2024) 35:1797**

A DLTS analysis of alpha particle irradiated commercial 4H-SiC Schottky barrier diodes

Mustafa A. M. Ahmed[1,2,*], F. D. Auret[3], J. M. Nel[3], and Andrè Venter[1]

[1] *Department of Physics, Nelson Mandela University, PO Box 77000, Gqeberha 6031, South Africa*
[2] *Department of Physics, Faculty of Education, University of Khartoum, PO Box 321, Omdurman, Sudan*
[3] *Department of Physics, University of Pretoria, Private Bag X20, Hatfield 0082, South Africa*

Received: 22 April 2024
Accepted: 8 September 2024
Published online:
25 September 2024

ABSTRACT

4H-SiC Schottky barrier diodes (SBDs) were exposed to 5.4 MeV alpha particles with fluences of 2.55× 10^{11} cm^{-2}, 5.11 × 10^{11} cm^{-2} and 7.67 × 10^{11} cm^{-2}, respectively. Transmission electron microscopy (TEM) and energy dispersive spectroscopy (EDS) was used to determine the structure and cross-sectional elemental composition of the device, while current–voltage and capacitance–voltage profiling were used to determine the primary electrical device-characteristics before and after irradiation. EDS revealed the presence of a <1 μm Ti layer, covered by 5 μm Al layer, in intimate contact with the SiC. Deep level transient spectroscopy (DLTS), performed in the temperature range 15–310 K, revealed one dominant peak around 50 K (E_c - 0.07 eV) in the unirradiated samples. This peak showed asymmetry suggesting that it may consist of more than one defect. Notably, $Z_{1/2}$, the carbon vacancy-related (V_c) defect commonly observed in as-grown *n*-type 4H-SiC, was not detected in the unirradiated reference sample. After irradiation, a broad peak emerged around 280 K (at 80 Hz), most likely $Z_{1/2,}$ having a shoulder around 180 K, was detected. Increasing the fluence resulted in a corresponding decrease in the concentration of the electron trap observed around 50 K (E_c - 0.07 eV), while the concentration increases for the defect detected around 280 K. Notably, the concentration of $Z_{1/2}$ was found to be strongly fluence dependent and linked to what we believe is a related to a silicon vacancy transition, labelled $S_{1/2}$ in literature. Laplace DLTS confirmed that the peak observed around 50 K is composed of multiple defects.

1 Introduction

In the absence of cost-effective diamond technology, SiC remains the semiconductor of choice for high-power electronic applications in extreme conditions. Although many SiC devices are commercially available, complete detail of their structure and performance under extreme conditions are often not provided in the manufacturer's specifications. The purpose of this study is to consider the effect of alpha particle radiation of varying fluences on the degradation of commercial SiC diodes.

Among the many SiC polytypes, 4H-, 6H-, and 3C-SiC (with bandgaps of 3.26 eV, 3.08 eV and 2.36 eV,

Address correspondence to E-mail: mustafa.sonbl@gmail.com

https://doi.org/10.1007/s10854-024-13507-2

respectively) are particularly significant for a wide range of power electronic and quantum technology applications. These polytypes due to their high breakdown field (approximately 10 times better than Si), thermal conductivity (at least double that of Si or GaAs) and radiation hardness, are ideal for high-power switching devices and UV-emitters and detectors operating in extreme environments [1–4]. The wide bandgap of 4H-SiC, roughly three times larger than silicon (Si), is a key advantage for this material. In addition to these extreme properties, 4H-SiC is preferred for bipolar devices [4], power electronics [5], and quantum sensing [6] applications mainly due to its high and isotropic mobility. Although other wide-bandgap semiconductors like GaN, ZnO, and SiC have also demonstrated potential for use in extreme environments, the development of high-purity homoepitaxial SiC layers with thicknesses exceeding 100 µm at reasonably low cost, favours this material over its competitors.

Crystal imperfections perturb the regular, periodic potential that electrons experience in a perfect crystal lattice. This disruption affects the solutions to the Schrödinger equation, which in turn modifies the energy states available to the electrons and therefore directly determine the optical and electronic properties of materials and the performance of related devices. These defects may be created intentionally or unintentionally during crystal growth and/or device fabrication processing. Additionally, doping by ion implantation is known to introduce secondary, unintended defects. In some cases, these defects can be beneficial. For instance, in the case of photo emitters it is desirable to have a high electron–hole recombination rate (i.e. short lifetime) which may be substantially enhance via deep-level centres. Conversely, these deep levels can reduce the lifetime of minority carriers by compensation effects leading to a decrease in the overall efficiency of detectors and solar cells, as it limits the time available for carriers to contribute to the desired electrical output. With regards to SiC, materials engineering, including defect manipulation, can serve as the basis for single-photon sources. Additionally, these defects can also facilitate the detection and manipulation of quantum states for quantum computing or quantum communication. Understanding and controlling defects in semiconductors therefore remain vitally important in our endeavour to advance materials and device engineering. Concerning radiation detectors, the study and characterizations of defects induced by alpha [7], proton [8], electrons [9] and neutrons irradiation damage in 4H-SiC are essential for the successful use of SiC in this technology [10–14].

In this study, deep-level transient spectroscopy (DLTS) and Laplace-DLTS were used to characterize defects introduced by 5.4 MeV α-particles in commercially available 4H-SiC Schottky diode. Current–voltage (*I-V*) and capacitance–voltage (*C-V*) measurements were used to study the effect of this irradiation on the primary diode characteristics.

2 Experimental details

4H-SiC Schottky barrier diode (SBD) chips, with part number CPW3-0600s003B, supplied by Cree Research Inc. (now trading as Wolfspeed), were used in this study. The anode and cathode, according to the supplier specifications, were Al (4 µm) and NiV/Ag (1.5 µm), respectively, while the dimensions of the chip are listed as 1.07 mm × 0.92 mm with a total SiC thickness of 377 µm. The zero-bias capacitance, measured at room temperature, is 155 pF while the DC blocking voltage is rated at 600 V. No additional information on the structure and the contact preparation conditions are available. Four chips were used in this study; a reference sample (Chip 1—no treatment) while Chips 2–4 were irradiated with α-particles, at room temperature, by positioning them directly on top of a ^{241}Am source for 10, 20 and 30 h, respectively, corresponding to fluences of 2.55×10^{11} cm^{-2}, 5.11×10^{11} cm^{-2} and 7.67×10^{11} cm^{-2}. An aside: americium-241 decays mainly via α-particle decay. Weak gamma rays (of no significance to this study) are produced as a by-product. The α-decay is shown as follows:

$$^{241}_{95}Am \rightarrow^{432.2y} {}^{237}_{93}Np + {}^{4}_{2}\alpha^{2+} + \gamma 59.54keV$$

On average, 85% of the α-particles decay with an energy of 5.486 MeV, 13% have energies of 5.433 MeV, while the remaining 2% have an energy of 5.388 MeV. After irradiation, all chips were mounted on patterned ceramic contact pads. Conducting silver paste was used to secure the ohmic contact (NiV/Ag) to the plate. Contact to the Al was made by bonding 33 µm gold wire to the contact pad using a TPT HB05 wire bonder. Figure 1. depicts the basic SBD structure and a TRIM calculation of the He^{++}-ion (α-particle) distribution. Incident high-energy particle may collide with host lattice atoms and, provided that this energy

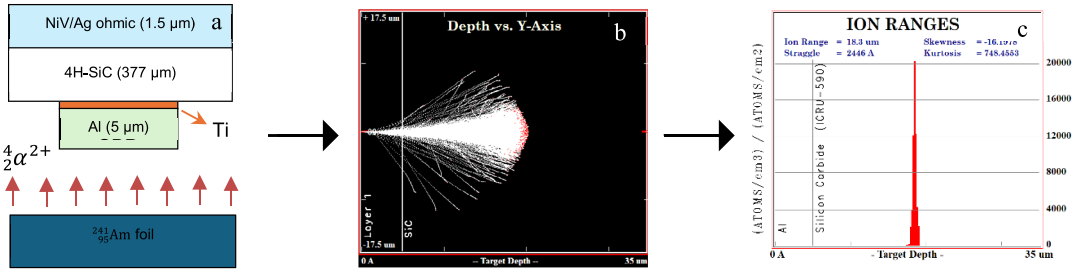

Fig. 1 **a** A schematic of the Cree SiC SBD used in this study and the 5.4 MeV americium-241 ($_{2}^{4}\alpha^{2+}$) irradiation to which it has been exposed. **b** A TRIM simulation of the ion distribution, following exposure to 10^6 events, predicts the creation of 160 vacancies/ion while in c) the target depth is estimated to be approximately 18.5 μm

exceeds the threshold displacement energy, a series of subsequent elastic collisions may result in a cascade of atomic displacements. Radiation damage is most frequently determined by calculating the number of displacements per atom following such a displacement cascade. Notably, in our experiment, the ion-stopping range is ~18 μm, substantially deeper that the accessible depletion region of the material, even with our extended bias capabilities available in our laboratory. It was therefore not possible to access the region where most of the vacancies would have been created, but we could observe the α-particle-induced near-surface damage.

3 Results and discussions

3.1 EDS TEM analysis

Figure 2 (a) depicts a cross-sectional energy-dispersive spectroscopy (EDS) scan of all the elements in the Cree SiC SBD (see inserted SEM cross section). The carbon layer, present at the surface, is attributed to a conductive coating evaporated onto the sample to prevent charging effects during the EDS measurement. Next, an Al layer, approximately 5 μm thick is detected. This is followed by a ~1 μm thick Ti layer on top of the SiC layer. No other metals are detected at the interface. We therefore assume that the Ti serves as the Schottky contact. A top view image of the SBD shows a ring around the Al contact which most likely serves as a guard ring, preventing side leakage between the anode and the cathode, an important design consideration especially in high power devices. Figure 2b depicts the bright field transmission electron microscopy (BF

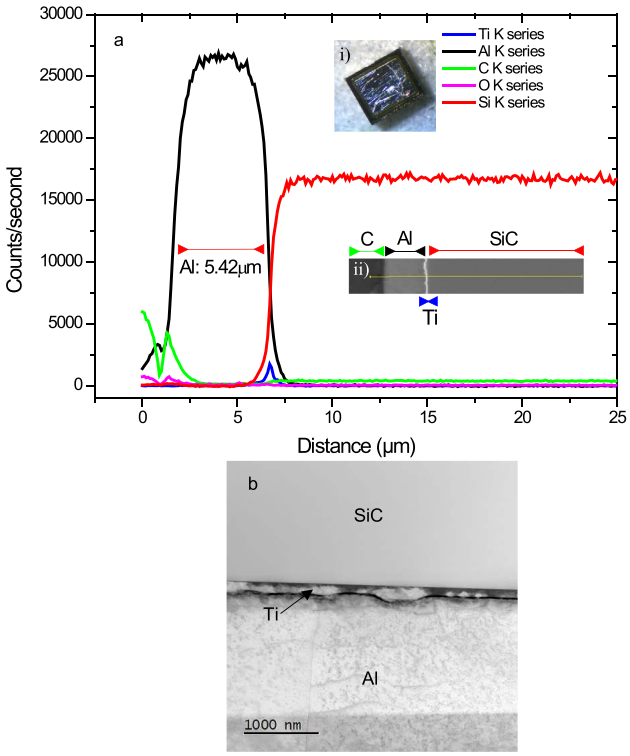

Fig. 2 **a** Cross-sectional energy-dispersive spectroscopy (EDS) scan of all the elements in the Cree SiC SBD. Notably, the Al (top) layer is approximately 5 μm thick. The insert i) is an optical image of the device while inset ii) shows a SEM cross-section of the area over which the EDS line scan was performed. **b** A BF-TEM image of the SiC/Ti/Al interface

TEM) image of the SiC/Ti/Al interface. A BF TEM shows interface region where the Ti layer lies between the SiC and the Al as seen by EDS (Fig. 2a).

Figure 3 shows cross-sectional, K-series EDS elemental mapping of the Cree SiC SBD. The map

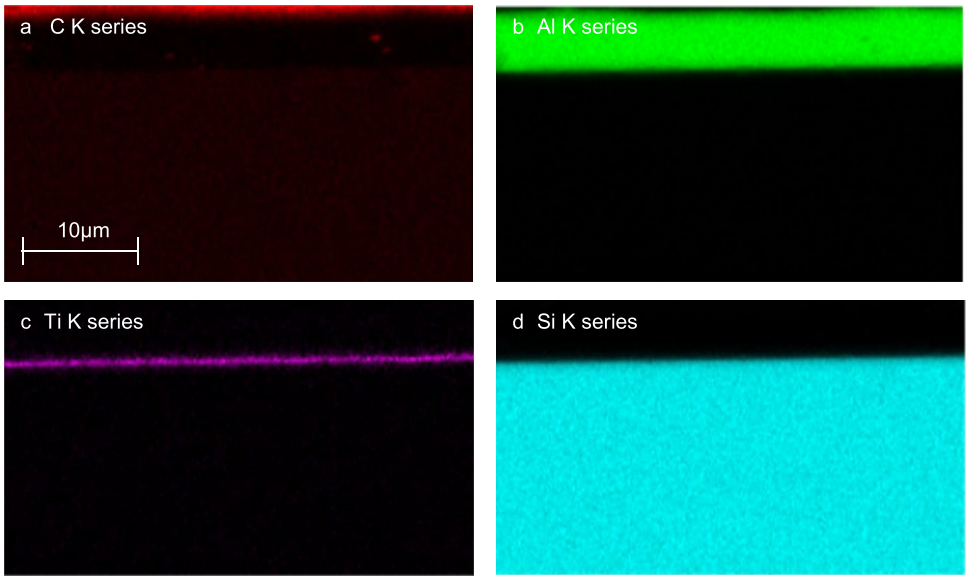

Fig. 3 Cross-sectional EDS elemental mapping of the Cree SiC SBD. The map confirms, **a** the presence of a carbon layer at the top surface, followed by, **b** a 5 μm thick Al layer and **c** a < 1 μm Ti layer. Also evident in **a** and **d** is the uniform distribution of C and Si in the SiC layer

confirms the presence of Al followed by a Ti layer in intimate contact with SiC. Expectedly, the presence of C (faint red spots), uniformly and stoichiometrically distributed in the SiC layer, is also visible. It is instructive to note that the work functions of Ti and Al are 4.33 eV and 4.20 eV, respectively, while the electron affinity of 4H-SiC is 3.10 eV. The theoretical barrier height $(\phi_b = \phi_m - \chi_S)$, suggests that Ti will be the better choice for metal–semiconductor barrier formation. For this reason, we believe that Ti serves as the Schottky barrier, while Al, in addition to other possible reasons, is added to "block" high-energy irradiation.

3.2 Current–voltage (*I-V*) characteristics

The current–voltage characteristics of a SBD for which the current across the barrier is predominantly due to thermionic emission is described by the following Eq. [15, 16]:

$$I(V) = I_s \exp\left(\frac{qV}{nkT}\right)\left[1 - \exp\left(-\frac{qV}{kT}\right)\right] \quad (1)$$

where V is the applied voltage, n, is the ideality factor, I_s, the saturation current, q, the elementary charge and k, Boltzmann's constant. For $V >> \frac{3kT}{q}$, which is the case for all the *I-V* measurements presented here, Eq. 1 reduces to:

$$I(V) = I_s \exp\left(\frac{qV}{nkT}\right) \quad (2)$$

The saturation current, I_s, is expressed as:

$$I_s = AA^*T^2 \exp\left(-\frac{q\phi_{IV}}{kT}\right) \quad (3)$$

where A is the cross-sectional area of the SBD, A^* is the effective Richard constant, and, ϕ_{IV}, the zero bias barrier height. The ideality factor, n, and the saturation current, I_s, is obtained from the slope and y-intercept, respectively, of a linearised plot using Eq. 2, while the barrier height is extracted from Eq. 3.

Figure 4. depicts room temperature (RT = 300 K) *I-V* characteristics of the reference (unirradiated) and 5.4 MeV alpha particle irradiated SiC SBDs. Notably, the exposure to radiation has little bearing on the forward current response while the reverse current decreases by approximately one order of magnitude.

Table 1 shows the primary *I-V*-derived SBD properties for both the reference and irradiated samples. The ideality factor of the unirradiated sample is 1.09, close to unity, implying that the current transport mechanism in this device can reasonably be attributed to thermionic emission. Following irradiation, no significant changes in the value of n or ϕ_{IV} were observed. The reverse bias current, measured at − 20 V, appears to decrease marginally upon irradiation, with the difference being approximately 1 order of magnitude between Chip 1

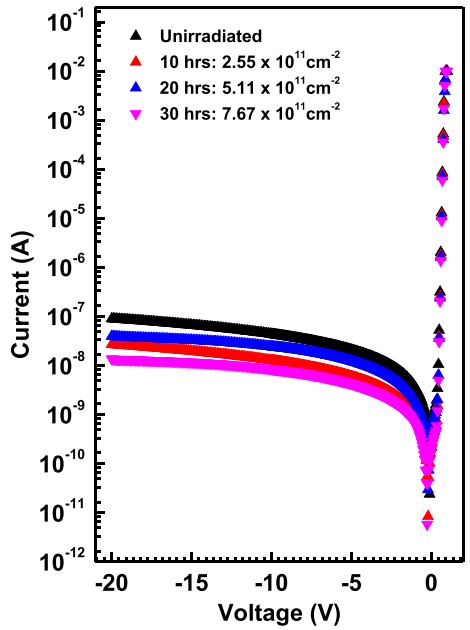

Fig. 4 RT (300 K) *I-V* characteristics of the reference and 5.4 MeV alpha particle irradiated SBDs for varying fluences

(unirradiated) and Chip 4 (irradiated for 30 h). The low and stable reverse current, ranging between 10^{-7} A and 10^{-8} A, confirms the quality and radiation hardness of the SBDs.

3.3 Capacitance–voltage (C-V) characteristics

The *C-V* relationship for a Schottky barrier diode is expressed as [16]:

$$\frac{1}{C^2} = \left(\frac{2}{\varepsilon_s q N_d A^2}\right)\left[V_{bi} - \frac{kT}{q} - V_a\right] \tag{4}$$

where ε_s is the permittivity of 4H-SiC, and V_a, the applied voltage. The x-intercept of a $\frac{1}{C^2} vs V$ plot gives V_0, which in turn is related to the built-in potential, V_{bi}, by the equation $V_{bi} = V_0 + kT/q$, where T is the measurement temperature. The *C-V*-derived barrier height, ϕ_{CV}, is given by [16–18]:

$$\phi_{CV} = V_{bi} + V_n + \frac{kT}{q} \tag{5}$$

with V_n being related by Eq. 6 to the density of states in the conduction band, N_c, and the free donor concentration, N_d.

$$V_n = \frac{kT}{q} \ln \frac{N_c}{N_d} \tag{6}$$

The derivative of Eq. 4 allows the determination of the free carrier depth profile [16]:

$$\frac{d}{dV}\left(\frac{1}{C^2}\right) = -2\left(\varepsilon_s q N_d A^2\right)^{-1} \tag{7}$$

Figure 5 depicts RT Mott-Schottky plots, performed at 1 MHz, together with the carrier concentration profiles for the reference and the irradiated SiC SBDs. Notably, in Fig. 5a, an increase in the alpha particle fluence is accompanied by a decrease in the device capacitance. This is most likely due to the formation of Si and C vacancy-related defects acting as electron traps [17, 19, 20]. The formation of these charge trapping centres, proportionate with the fluences to which the chips were exposed, is also evident in the free carrier depth profiles depicted in Fig. 5b, with the lowest free carrier concentration observed for Chip 4, receiving the highest fluence [21]. The material and device properties, derived from the *C-V* measurements, are listed in Table 1.

The removal rate of the free carrier concentration (η) due to compensation is determined by:

$$\eta = \frac{\Delta N}{\varphi} \tag{8}$$

Where ΔN and φ, respectively, are the change in the free carrier concentration before and after irradiation, and the fluence at which the SiC SBDs were irradiated

Table 1 Primary *I-V* and *C-V* derived characteristics of the unirradiated and α-particle irradiated SiC diodes using varying fluences

SiC-SBDs	*I-V* analysis			*C-V analysis*		
	n	$\phi_{B(I\text{-}V)}$ (eV)	$I_{reverse}$(A) at (-20 V)	N_d (cm^{-3})	$\phi_{B(C\text{-}V)}$ (eV)	V_{bi} (V)
Chip 1 (unirradiated)	1.09	1.15	1.0×10^{-7}	1.7×10^{16}	1.81	1.64
Chip 2 (2.55×10^{11} cm^{-2})	1.08	1.13	2.6×10^{-8}	1.3×10^{16}	1.88	1.70
Chip 3 (5.11×10^{11} cm^{-2})	1.15	1.10	3.8×10^{-8}	1.2×10^{16}	2.44	2.26
Chip 4 (7.67×10^{11} cm^{-2})	1.08	1.14	1.2×10^{-9}	8.0×10^{15}	3.56	3.37

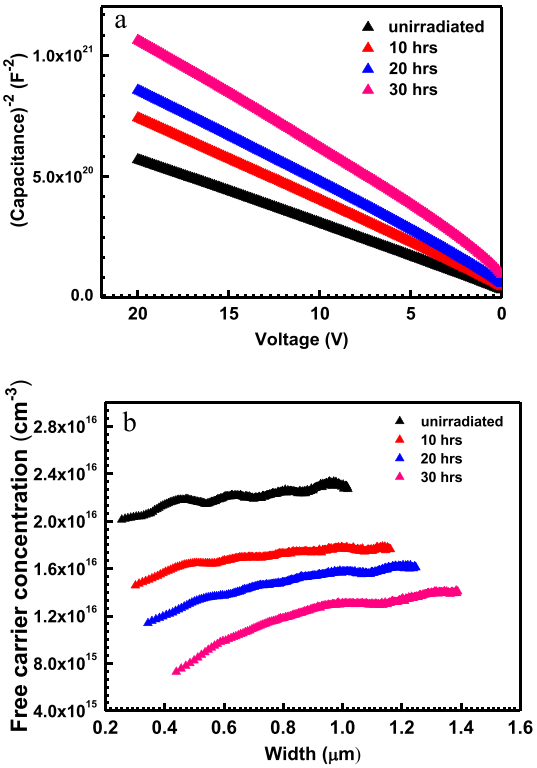

Fig. 5 **a** RT Mott-Schottky plots, performed at 1 MHz, **b** subsequently calculated free carrier depth profiles of the reference and irradiated SiC SBDs

[22–24]. Generally, the carrier removal rate decreases with increasing α-particle fluence. Higher fluence normally increases the formation of point defects, but it may also cause complex interactions among defects, which might result in a decreased carrier removal rate at very high fluences. For Chips 2–4, η were 2.3×10^4 cm^{-1}, 1.6×10^4 cm^{-1} and 1.3×10^4 cm^{-1}, respectively.

The fluence-dependent free carrier removal rate in our experiments is roughly one order of magnitude higher than that reported for Ni/4H-SiC Schottky diode devices also irradiated with 5.4 MeV alpha particles in the fluence range 2.2×10^{10}–9.2×10^{11} cm^{-2} [19], [20]. The most likely explanation for this observation is that the thinner (Ni) metal layer [19], resulted in lower concentrations of near-surface damage, given that the ion range would extend deeper into the material in this case.

The barrier height obtained from *I-V* measurements are nearly constant for all fluences as is that, although slightly higher, obtained from *C-V* measurements (see Table 1). Figure 5b shows the free carrier depth profiles of the unirradiated and α-particle irradiated SiC SBDs Chips, measured at 300 K employing a reverse bias of − 20 V. As is evidenced, the free carrier concentration decreased with increasing α-particle fluences. As already stated, this decrease is most likely due to the capture of free charge by vacancy-related defects, mostly Frenkel pairs caused by the irradiation.

3.4 Deep-level Transient Spectroscopy

Particle irradiation, in addition to creating point defects, typically increases the concentration of native defects and therefore enables a detailed study of their formation dynamics, properties, and the effects on the optical and electronic properties of semiconductors. Two dominant recombination centres, labelled in literature as $Z_{1/2}$ and $EH_{6/7}$, assigned to different charge state transitions of the carbon vacancy (V_C), are commonly observed in as-grown *n*-type 4H-SiC by DLTS [20, 22]. The $Z_{1/2}$ defect exhibits a negative-U behaviour, meaning it has a negative correlation energy. This implies that the defect level captures two electrons, and the energy required to capture the second electron is larger than the energy required to capture the first. In general, the concentration of these defects depends on the growth temperature and the C/Si ratio. It has been reported that carbon-rich conditions and lower growth temperatures impede the formation of these defects leading to the belief that they are likely related to carbon vacancies. [23] Importantly, $Z_{1/2}$ and $EH_{6/7}$ have been identified as non-radiative minority carrier lifetime killing centres, which is critical for the performance of electronic and optoelectronic devices [24]. It is instructive to note that defects created by α-particle irradiation may also be produced by high-energy electron irradiation. Pastuovic et al. detected EH_1, EH_3, EH_4 and EH_5 in 4H-SiC following 2 MeV He^{2+} and 600 keV H^+ irradiation [25]. Although $EH_{1/3}$ were thought to be the same defect as $S_{1/2}$, (labelled as such following fast neutron irradiation), Alfieri and Mihaila demonstrated that $EH_{1/3}$ and $S_{1/2}$ are unrelated. Specifically, $EH_{1/3}$ is the same defect in different charge states, related to the carbon interstitial (C_i) in SiC. These defects are introduced exclusively through low-energy electron irradiation (< 200 keV) where silicon atoms cannot be displaced, meaning the defects are related to displacements or interactions involving carbon atoms [17]. $S_{1/2}$ have been identified as silicon-vacancy related charge states and are therefore only

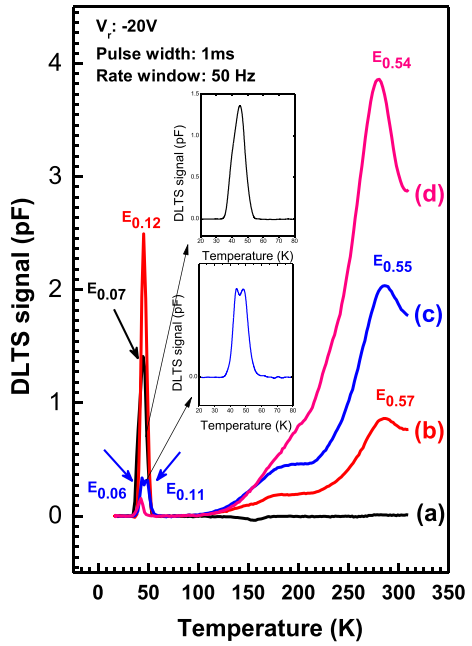

Fig. 6 DLTS spectra of **a** the reference, and **b–d**, the α-particle irradiated SiC SBDs receiving fluences of 2.55×10^{11} cm^{-2} (10 h), 5.11×10^{11} cm^{-2} (20 h) and 7.67×10^{11} cm^{-2} (30 h), respectively. The inset figures show the asymmetry (top) of the peak detected around 50 K for the reference sample, while the separation of closely spaced defects similar but resolvable emission rates (bottom) is also evident

observed for electron irradiation energies > 200 keV [21].

Figure 6. depicts conventional DLTS spectra of the reference and irradiated SiC SBDs. The measurements were acquired in the 15–310 K range, using a reverse bias of -20 V, a pulse width of 1 ms and a rate window of 50 Hz.

As shown in Fig. 6, only one defect ($E_{0.07}$) was observed around 50 K in the unirradiated (reference) SiC SBD. Conspicuously, no evidence for the presence of $Z_{1/2}$, was observed in the reference sample. Note that the peak around 50 K is asymmetric (top inset figure), implying that it may be composed of more than one defect with similar emission rates. Following irradiation, two prominent defects at approximately 180 K and 280 K emerged. Notably, the intensity of both these peaks increased with an increase in fluence. The formation rate of the peak at ~280 K is the largest, suggesting that this specific defect is being created more rapidly or abundantly compared to other. This assertion is of course made on the premise that optimal pulse conditions were used to fill and subsequently detect these defects. This increase implies that the defect concentration correlates with the incident particle fluence, most likely due to the formation of vacancy-related defects (24). It is instructive to note that the intensity of the peak around 50 K in Chip 2, following 10 h of irradiation, increased by a factor of ~2. The shift was accompanied by an increase in the activation energy from 0,07 eV to 0,12 eV. Increasing the fluences further (Chips 3 and 4) resulted in a progressive decrease in the capacitance signal, and hence this (~50 K) defect's concentration, with clear evidence that this peak in Chip 3 (irradiated for 20 h) has two constituents, as is depicted in Fig. 6c (insert 2). Interestingly, upon comparing curves (b), (c) and (d) in Fig. 6, it is obvious that the intensity of the peak at ~ 50 K is inversely correlated with the peak observed around ~280 K. The anomalous increase in the intensity of the peak ~50 K, following the first irradiation, is tentatively attributed to the pinning of the Fermi level related to surface damage. The activation energy of this defect, E_c - 0.12 eV, compares well with reported values for Ti. Recall, from the EDS results, that the SBDs consisted of Ti, in intimate contact with the SiC. We, therefore, speculate that the increase may be attributed to the in-diffusion of the Ti, aided by the impinging 5.4 MeV alpha particles.

Table 2 Electronic properties of defects detected by conventional DLTS in the reference and 5.4 MeV α-particle irradiated SiC SBDs. The peak positions were obtained using a rate window of 50 Hz

Defects	E_T (eV)	$\sigma_{napparent}(cm^2)$	T (K)	Defect ID	References
$E_{0.07}$ spectrum (a)	$E_C - 0.07$	4.14×10^{-15}	44.85	N_i	[28, 29]
$E_{0.12}$ spectrum (b)	$E_C - 0.12$	3.50×10^{-9}	45.46	Ti	[26, 27]
$E_{0.06}$ spectrum (c)	$E_C - 0.06$	2.25×10^{-15}	43.85	N_i	[28, 29]
$E_{0.10}$ spectrum (d)	$E_C - 0.10$	4.86×10^{-11}	44.23	N_i	[28, 29]
$E_{0.11}$ spectrum (c)	$E_C - 0.11$	8.94×10^{-11}	49.50	Ti	[30]
$E_{0.57}$ spectrum (b)	$E_C - 0.57$	4.85×10^{-14}	277.42	V_c (Z_1/Z_2)	[31, 32]
$E_{0.55}$ spectrum (c)	$E_C - 0.56$	1.64×10^{-14}	283.40	V_c (Z_1/Z_2)	[31, 32]
$E_{0.54}$ spectrum (d)	$E_C - 0.53$	4.47×10^{-15}	286.00	V_c (Z_1/Z_2)	(32)

Table 2 presents the electronic properties, determined by conventional DLTS, of the defects detected before and after alpha particle irradiation. The activation energy, E_T, and the apparent capture cross-section, σ_a, for these defects were obtained from the slope and intercept, respectively, of a T^2/e_n vs $1000/T$ Arrhenius plot, using rate windows ranging between 5 and 500 s^{-1}. Notably, we could not resolve the defect signature of the peak around 180 K by either conventional or Laplace DLTS because of the large emission rate overlap of a seemingly continuum of defect states between ~180 K and 280 K. Paradzah et al. [26, 27] observed a similar defect when in their 4H-SiC Schottky diodes irradiated with 5.4 MeV alpha particles and attributed the defect level to the presence of titanium impurities.

Defect levels in 4H-SiC with activation energies ranging between 0.06 eV and 0.10 eV have previously been attributed to nitrogen occupying vacant carbon sites in 4H-SiC [33, 34]. The defect levels $E_{0.55–0.57}$ presented in curves b–d in Fig. 4 are attributed to the well-reported $Z_1/_2$ defect in SiC, the double negative and neutral, V_c(= /0), charge states of the carbon vacancy [31, 35, 36]. It is believed that these defect levels are related to a "family" of closely spaced defects and are similar to $E_{0.62}$ and $E_{0.67}$ reported for $Z_{1/2}$ by Kimoto et al. [34], with the dominant being the silicon interstitial or a di-carbon pair complexed with a nitrogen atom. A similar defect was observed in 6H-SiC by Polyakov et al.[37] which these authors also attributed to intrinsic carbon vacancies. It should be noted that the defect energies reported for $Z_{1/2}$ (~285 K) in our study were obtained using multi-rate window conventional DLTS. The shift in peak position with fluence, and therefore the defect energy, is attributed to the neighbouring defect most likely $S_{1/2}$ appearing as a shoulder on the low-temperature side of the spectrum. Arrhenius plots of the defects observed are depicted in Fig. 7.

3.5 Laplace -DLTS

The defects observed in Chip 3 and Chip 4, using conventional DLTS, were further analysed using high-resolution Laplace DLTS. Laplace DLTS, given a signal-to-noise ratio > 1000 and a temperature stability of ± 20 mK, can resolve defects with an emission rate ratio (e_1/e_2) as low as 2. This translates to a ~ 2 meV energy resolution at 100 K. Figure 8a shows Laplace-DLTS spectra for Chip 3, measured between 50 and

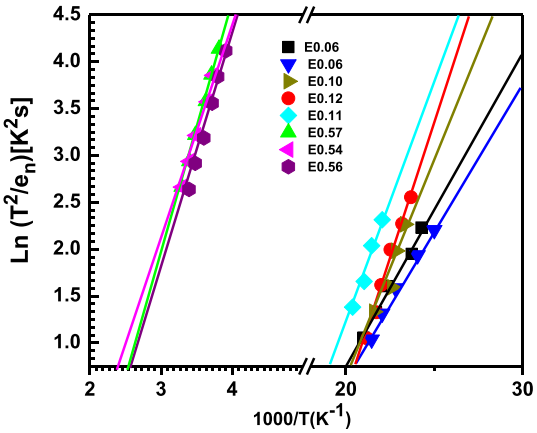

Fig. 7 Arrhenius plots of the unirradiated and alpha particle irradiated chips devices obtained from DLTS

52 K. While only two defects were resolved with conventional DLTS, Laplace DLTS suggests that the peak may consist of three components. The activation energies of the constituent are 0.08 eV, 0.10 eV and 0.14 eV, in reasonable agreement with that obtained using conventional DLTS.

Furthermore, the measured apparent capture cross-sections σ_a for the defect levels, are 1×10^{-13} cm^2, 1×10^{-12} cm^2 and 3×10^{-9} cm^2, respectively. Figure 8b shows Laplace-DLTS spectra for Chip 4, receiving the highest fluence, obtained in the temperature range 47–49 K. We only observed two defects here, $E_{0.08}$ and $E_{0.10}$ (see Fig. 4b), with an apparent capture cross-section of 6.4×10^{-14} cm^2 and 2×10^{-13} cm^2, respectively.

Figure 9 depicts Arrhenius plots using LDLTS for the defects observed in Chip 3 and Chip 4, irradiated for 20 Hours and 30 h respectively. Clearly, three defects with activation energies of 0.08 eV, 0.10 eV and 0.14 eV could be resolved. These activation energies values are in close agreement with that obtained using conventional DLTS. The measured apparent capture cross sections σ_a for the defect levels $E_{0.08}$, $E_{0.10}$ and $E_{0.14}$ are 1×10^{-13} cm^2, 1×10^{-12} cm^2 and 3×10^{-9} cm^2, respectively. As suggested in Fig. 8b only two defects, $E_{0.08}$ and $E_{0.10}$ (see Fig. 8b), with apparent capture cross-sections of 6.4×10^{-14} cm^2 and 2×10^{-13} cm^2 were detected.

4 Conclusion

Commercially sourced 4H-SiC Schottky barrier diodes were irradiated with 5.4 MeV α-particles using varying fluences. The reverse bias current was

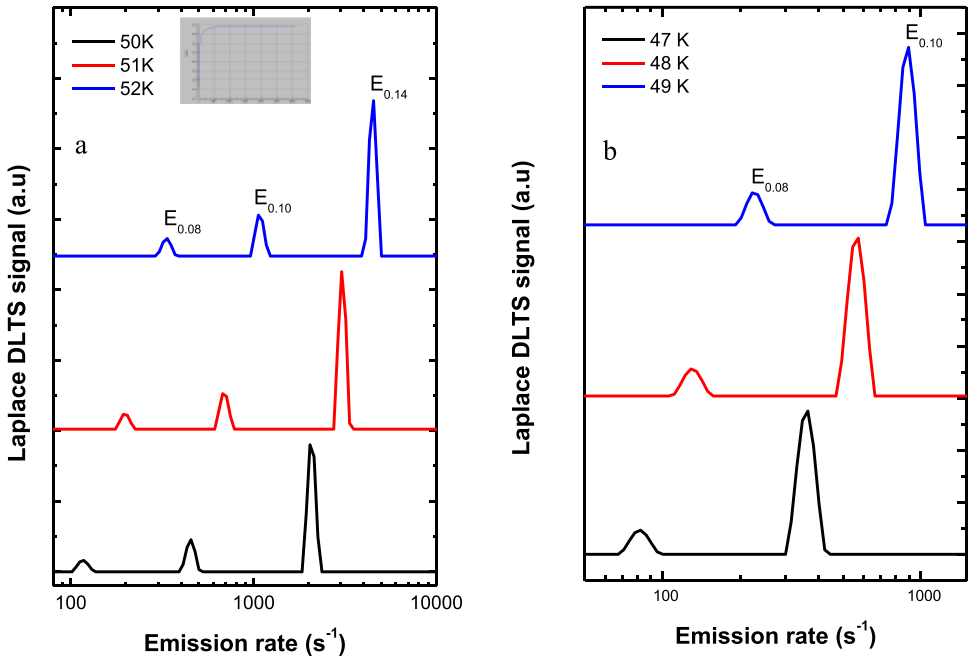

Fig. 8 Laplace DLTS spectra of **a** Chip 3 and **b** Chip 4 performed in the temperature range 50–52 K and 47–50 K respectively. Spectra were acquired at a reveres bias of −20 V. The filling pulse was 20 V and the pulse width, 1 ms

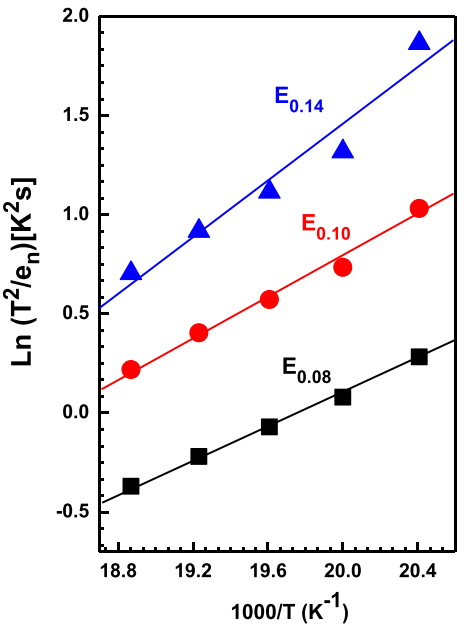

Fig. 9 Arrhenius plots for the Laplace-DLTS-determined emission rates for the decomposed peak detected around 50 K

measured at -20 V before and after irradiation and showed only a marginal decrease upon irradiation suggesting a high degree of radiation hardness in the Cree 4H-SiC SBDs. Capacitance–Voltage (*C-V*) depth profiling confirms a reduction in free carrier concentration, consistent with the α-particle fluence received. This reduction is attributed to the formation of charge compensation deep-level centres introduced by the irradiation. Deep-Level Transient Spectroscopy (DLTS) revealed a single defect, $E_{0.07}$ (~ 50 K), in the reference sample. Nitrogen is a common dopant in SiC, and this defect is, therefore, likely related to nitrogen incorporation during crystal growth as has been been reported. The inverse correlation between the carrier removal rate and fluence suggests that, in addition to simple point defects being formed, complex defect interactions should be expected. Indeed, following irradiation, DLTS revealed the presence of several defects following irradiation, among them $Z_{1/2}$ (~280 K), accompanied by the simultaneous emergence of a defect around ~180 K. Unfortunately, the smearing out of the defect and its "integration" with $Z_{1/2}$ made it difficult to extract its trap signatures with absolute certainty. Given the energy (5.4 MeV) of the radiation used in this study and the trap signatures presented in Table 2, we tentatively assign this defect to silicon vacancies—specifically, the commonly reports trap, $S_{1/2}$, attributed to $V_{Si}(-3/=)$ and $V_{Si}(=/-)$ transitions. Pastuovic et al. following 2 MeV He^{2+} and 600 keV H^+ irradiation observed similar DLTS results. Notably for both these defects the concentrations increased with the received α-particle fluences. Both the $E_{0.55–0.57}$ and the suspected $S_{1/2}$ defects

show an increase in concentration with increase in α-particle fluence, indicating a direct relationship between irradiation dose and defect formation.

Following exposure for 10 h the concentration of the defect around 50 K increased by a factor of ~2 and shifted upward in energy from $E_{0.07}$ to $E_{0.12}$ in agreement with reported values for a Ti-related defect in 4H-SiC. This is not unexpected since the presented EDS results confirmed Ti as the anode metal in these devices.

Acknowledgements

The authors gratefully acknowledge: Nelson Mandela University (NMU), South Africa, for their financial support. Center for High Resolution TEM at the NMU for their assistance with the TEM and EDS analyses.

Author contributions

MA: Acquired and analysed the data, writing the original draft of the manuscript. FDA: acquired the data, review and editing the manuscript. JN: review and editing the manuscript. AV: Supervision, review, editing the manuscript and approve the final version of the manuscript.

Funding

Open access funding provided by Nelson Mandela University. The authors have not disclosed any funding.

Data availability

Data used in this study will be available upon request from the corresponding author.

Declarations

Conflict of interest The authors declare that they have no known competing financial interests or personal relationships that could have appeared to influence the work reported in this paper.

Ethical approval Not applicable.

Consent to participate Not applicable.

Consent for publication Not applicable.

References

1. Z. Tong, L. Gu, Z. Ye, K. Surakitbovorn, J. Rivas-Davila, On the techniques to utilize SiC power devices in high-and very high-frequency power converters. IEEE Trans. Power Electron. **34**(12), 12181–12192 (2019)
2. T. Wejrzanowski, E. Tymicki, T. Plocinski, J.J. Bucki, T.L. Tan, Design of SiC-doped piezoresistive pressure sensor for high-temperature applications. Sensors **21**(18), 6066 (2021)
3. J.A. Cooper, D.T. Morisette, Performance limits of vertical unipolar power devices in GaN and 4H-SiC. IEEE Electron. Device Lett. **41**(6), 892–895 (2020)
4. S. Zhao, X. Zhao, Y. Wei, Y. Zhao, H.A. Mantooth, A review of switching slew rate control for silicon carbide devices using active gate drivers. IEEE J. Emerg. Sel. Top Power Electron. **9**(4), 4096–4114 (2020)
5. D. Puglisi, G. Bertuccio, Silicon carbide microstrip radiation detectors. Micromachines **10**(12), 835 (2019)
6. T.M. Hoang, H. Ishiwata, Y. Masuyama, Y. Yamazaki, K. Kojima, S.Y. Lee et al., Thermometric quantum sensor using excited state of silicon vacancy centers in 4H-SiC devices. Appl Phys Lett. (2021). https://doi.org/10.1063/5002760

7. I. Capan, R. Bernat, T. Makino, T. Knežević, 4H-SiC Schottky barrier diodes as radiation detectors: a role of Schottky contact area. Diam Relat Mater **137**, 110072 (2023)
8. Y.X. Lin, D.S. Chao, J.H. Liang, J.Y. Jiang, C.F. Huang, Electrical deterioration of 4H-SiC MOS capacitors due to bulk and interface traps induced by proton irradiation. Microelectron. Reliab. **142**, 114927 (2023)
9. M. Xiang, D. Wang, M. He, G. Rui, Y. Ma, X. Zhu et al., Electrical characterization and temperature reliability of 4H-SiC Schottky barrier diodes after Electron radiation. Microelectron. Reliab. **141**, 114886 (2023)
10. K.C. Mandal, S.K. Chaudhuri, R. Nag, High performance Pd/4H-SiC epitaxial schottky barrier radiation detectors for harsh environment applications. Micromachines **14**(8), 1532 (2023)
11. A. Siddiqui, A. Hallén, A. Hussain, M. Usman, Carrier removal rates in 4H–SiC power diodes–A predictive analytical model. Mater. Sci. Semicond. Process. **167**, 107771 (2023)
12. K.C. Mandal, S.K. Chaudhuri, F.H. Ruddy, High-resolution alpha spectrometry using 4H-SiC detectors: a review of the state-of-the-art. IEEE Trans. Nucl. Sci. (2023). https://doi.org/10.1109/TNS.2023.3267996
13. O. Karadavut, J.W. Kleppinger, S.K. Chaudhuri, K.C. Mandai, Effect of enhanced hole transport on the performance of Ni/Y 2 O 3/n-4H-SiC Epilayer radiation detectors. IEEE Trans. Nucl. Sci. (2023). https://doi.org/10.1109/TNS.2023.3306276
14. Rafi JM, Pellegrini G, Godignon P, Rius G, Dauderys V, Tsunoda I, et al. Low Temperature Annealing of Electron, Neutron and Proton Irradiation Effects on SiC Radiation Detectors. IEEE Trans Nucl Sci. 2023;
15. S.M. Sze, Y. Li, K.K. Ng, *Physics of semiconductor devices* (John wiley & sons, New York, 2021)
16. E.H. Rhoderick, R.H. Williams, *Metal-semiconductor contacts*, vol. 129 (Clarendon press Oxford, Oxford, 1988)
17. G. Alfieri, A. Mihaila, Isothermal annealing study of the EH1 and EH3 levels in n-type 4H-SiC. J. Phys. Condens. Matter **32**(46), 465703 (2020)
18. F.D. Auret, S.A. Goodman, M. Hayes, M.J. Legodi, H.A. van Laarhoven, D.C. Look, Electrical characterization of 1.8 MeV proton-bombarded ZnO. Appl. Phys. Lett. **79**(19), 3074–6 (2001). https://doi.org/10.1063/1.1415050
19. E. Omotoso, W.E. Meyer, F.D. Auret, A.T. Paradzah, M. Diale, S.M.M. Coelho et al., Effects of 5.4MeV alpha-particle irradiation on the electrical properties of nickel Schottky diodes on 4H–SiC. Nucl. Instrum. Methods Phys. Res. B **365**, 264–8 (2015)
20. T. Dalibor, G. Pensl, H. Matsunami, T. Kimoto, W.J. Choyke, A. Schöner et al., Deep defect centers in silicon carbide monitored with deep level transient spectroscopy. Phys. Status Solidi (a). **162**(1), 199–225 (1997)
21. M.E. Bathen, A. Galeckas, J. Müting, H.M. Ayedh, U. Grossner, J. Coutinho et al., Electrical charge state identification and control for the silicon vacancy in 4H-SiC. npj Quantum Inf. **5**(1), 111 (2019)
22. C. Hemmingsson, N.T. Son, O. Kordina, J.P. Bergman, E. Janzén, J.L. Lindström et al., Deep level defects in electron-irradiated 4H SiC epitaxial layers. J. Appl. Phys. **81**(9), 6155–6159 (1997)
23. L. Storasta, J.P. Bergman, E. Janzén, A. Henry, J. Lu, Deep levels created by low energy electron irradiation in 4H-SiC. J. Appl. Phys. **96**(9), 4909–4915 (2004)
24. X. Gao, X. Wang, Y. Li, Z. Yang, M. Gong, M. Huang et al., Comparing the effect between room temperature and low temperature heavy ion irradiation by deep level transient spectroscopy. Nucl. Instrum. Methods Phys. Res. B **550**, 165319 (2024)
25. Ž Pastuović, R. Siegele, I. Capan, T. Brodar, Sato S. Ichiro, T. Ohshima, Deep level defects in 4H-SiC introduced by ion implantation: the role of single ion regime. J. Phys. Condensed Matter. **29**(47), 475701 (2017)
26. A.T. Paradzah, F.D. Auret, M.J. Legodi, E. Omotoso, M. Diale, Electrical characterization of 5.4MeV alpha-particle irradiated 4H-SiC with low doping density. Nucl. Instrum. Methods Phys. Res. B **358**, 112–6 (2015)
27. N. Achtziger, W. Witthuhn, Band gap states of Ti, V, and Cr in 4H–silicon carbide. Appl. Phys. Lett. **71**(1), 110–2 (1997). https://doi.org/10.1063/1.119485
28. T. Kimoto, A. Itoh, H. Matsunami, S. Sridhara, L.L. Clemen, R.P. Devaty et al., Nitrogen donors and deep levels in high-quality 4H–SiC epilayers grown by chemical vapor deposition. Appl. Phys. Lett. **67**(19), 2833–2835 (1995)
29. E. Omotoso, W.E. Meyer, E. Igumbor, T.T. Hlatshwayo, A.R.E. Prinsloo, F.D. Auret et al., DLTS study of the influence of annealing on deep level defects induced in xenon ions implanted n-type 4H-SiC. J. Mater. Sci. Mater. Electron. **33**(19), 15679–88 (2022). https://doi.org/10.1007/s10854-022-08471-8
30. A.A. Lebedev, Deep level centers in silicon carbide: a review. Semiconductors **33**(2), 107–30 (1999). https://doi.org/10.1134/1.1187657
31. E. Omotoso, W.E. Meyer, F.D. Auret, A.T. Paradzah, M.J. Legodi, Electrical characterization of deep levels created by bombarding nitrogen-doped 4H-SiC with alpha-particle irradiation. Nucl. Instrum. Methods Phys. Res.B **371**, 312–6 (2016)

32. T. Dalibor, G. Pensl, H. Matsunami, T. Kimoto, W.J. Choyke, A. Schöner et al., Deep defect centers in silicon carbide monitored with deep level transient spectroscopy. Phys. Status Solidi A Appl. Res. **162**(1), 199–225 (1997)
33. C.Q. Chen, J. Zeman, F. Engelbrecht, C. Peppermüller, R. Helbig, Z.H. Chen et al., Photothermal ionization spectroscopy of shallow nitrogen donor states in 4H–SiC. J. Appl. Phys. **87**(8), 3800–5 (2000). https://doi.org/10.1063/1.372417
34. T. Kimoto, A. Itoh, H. Matsunami, S. Sridhara, L.L. Clemen, R.P. Devaty et al., Nitrogen donors and deep levels in high-quality 4H–SiC epilayers grown by chemical vapor deposition. Appl. Phys. Lett. **67**(19), 2833–5 (1995). https://doi.org/10.1063/1.114800
35. L. Zhao, Y. Tang, Y. Bai, M. Qiu, Z. Wu, Y. Yang et al., Analysis of defects and electrical characteristics of variable-temperature proton-irradiated 4H-SiC JBS diodes. Electronics **11**(9), 1341 (2022)
36. I. Capan, T. Brodar, J. Coutinho, T. Ohshima, V.P. Markevich, A.R. Peaker, Acceptor levels of the carbon vacancy in 4H-SiC: combining Laplace deep level transient spectroscopy with density functional modeling. J. Appl. Phys. **124**(24), 245701 (2018). https://doi.org/10.1063/1.5063773
37. A.Y. Polyakov, Q. Li, S.W. Huh, M. Skowronski, O. Lopatiuk, L. Chernyak et al., Minority carrier diffusion length measurements in 6H-SiC. J Appl Phys. (2005). https://doi.org/10.1063/11853501